

Computational screening for clathrates among predicted crystal structures

Jonas Nyman^{1,2,✉}, Graeme M. Day³, and Peter Ahlström⁴

¹The Cambridge Crystallographic Data Centre, 12 Union Road, Cambridge CB2 1EZ, UK; jnyman@ccdc.cam.ac.uk

²Holly Chemistry AB, Hangarvägen 13, 69135 Karlskoga, Sweden; Tel: +46 793261665

³School of Chemistry, University of Southampton, University Rd, Southampton SO17 1BJ, UK; Tel: +44 2380599174; E-mail: g.m.day@soton.ac.uk

⁴Faculty of Textiles, Engineering and Business, University of Borås, Allégatan 4, 50190 Borås, Sweden

We present a computational study of gas adsorption in a large set of predicted porous organic molecular crystal structures. A large number of computer-generated porous crystal structures of *o*- and *m*-fluorophenol, resorcinol and triptycene trisbenzimidazolone were screened for their ability to adsorb xenon, carbon dioxide and methane, and thereby form clathrates. The thermodynamic driving force for gas adsorption was calculated with rigid-body lattice dynamics and grand canonical Monte Carlo simulations, using an accurate anisotropic force field with electrostatic multipoles. The results suggest that the studied compounds may form several clathrate structures at mild temperatures and pressures, which may facilitate carbon capture or separation of gases by molecular sieving.

Crystal structure prediction | clathrates | porous materials | carbon capture
Correspondence: jnyman@ccdc.cam.ac.uk

Introduction

Clathrates are crystalline materials consisting of a porous framework, built up by discrete molecules, that adsorb guest molecules in their pores (1–3). The framework acts as a host for the relatively weakly bound gaseous guests.

In the absence of directional interactions between molecules, and disregarding lattice vibrations, the densest crystal structure of any given composition is the most stable one (4, 5). Consequently, the empty host frameworks are generally unstable and clathrates are rare (6, 7).

Hydroquinone is one of the few widely known clathrate-forming molecules (8). It has been extensively studied both experimentally and computationally. Hydroquinone easily forms clathrates with a large number of guests, including CO₂ under mild pressure (9). The hydroquinone H₂ clathrate was found experimentally only after a computational study predicted that such clathrates can form and that they may have more than one H₂ molecule in each pore (10), obviously of great interest for gas storage applications. The computational predictions have since been confirmed; the clathrate exhibits fast and reversible adsorption of hydrogen gas at room temperature and has double and triple occupancy of H₂ at elevated pressures (11, 12). In addition, the demonstrated separation of ethane/methane and CO₂/N₂ gas mixtures by hydroquinone clathrate is another example of a potential industrial application (13, 14).

Phenol and several *para*-substituted phenol derivatives are known to readily form clathrates with various gases at low temperatures, and because of their selective affinities for dif-

ferent guests, they can be used for gas separation (15). Phenols with substitutions at the *ortho*- and *meta*-positions are less prone to forming clathrates, but *o*- and *m*-fluorophenol xenon clathrates have been described (16–18).

Clathrates with a host framework of water molecules, commonly called clathrate hydrates, have been intensively studied because of the problems they cause during off-shore petroleum and natural gas extraction (19). The goal has then often been to avoid the formation of a water methane clathrate. More recently, additives that induce the formation of clathrate hydrates have been studied as a means to capture CO₂ from flue gas or for separating CO₂ from biogas pre-combustion (20).

Computational studies of clathrates have mainly focused on the calculation of guest adsorption energies by traditional force field methods. The adsorption energy is calculated either from the static lattice energy (21, 22), or with methods that consider the dynamics and generate a thermodynamic ensemble, such as molecular dynamics or Monte Carlo (MC) simulations (23–25). Lattice dynamics is an alternative to these methods, and can be performed with more accurate force fields (26, 27), and at a moderate computational cost. Lattice dynamics studies of clathrates are rare, but Dang and Pettitt (28) and Belosludov *et al.* (29) performed lattice dynamics on hydroquinone clathrates with several guest molecules and compared the computationally obtained vibrational frequencies to experimental data. Conventional lattice dynamics does however rest on an assumption that the molecules are fixed in the crystal structures and only vibrate harmonically around their equilibrium positions, which is often an adequate approximation for close-packed molecular crystals (30, 31), but probably less so for clathrates, as the guest molecules have a rattling motion in the cavities, rather than a vibrational one (32–34).

The adsorption of gases in clathrates depend on both an enthalpic (static) binding energy, and an entropic part that depends on the guest molecules' motion, and how the presence of the guest affects the motion of the host framework. The ideal cavity size thus provides a balance of binding enthalpy (favouring a tight fit) and entropy (allowing the guest to move). Several researchers have noted this careful balance, and how the binding affinity of a guest in a host is related to the guest-to-cavity volume ratio (35–37). The guest-to-cavity volume ratio, or the guest's packing coefficient, is hence an important property of clathrates. Maximal affinity

occurs when the volume ratio is close to 55% (38), *i.e.* substantially less than close-packed.

Crystal structure prediction (CSP) generates hundreds of hypothetical crystal structures in an 'energy landscape' (39). The main purpose of CSP has so far been about finding the most stable form and possibly a few metastable polymorphs, a few kJ/mol above the global minimum (40). Recently however, we have seen a change in the focus of some CSP studies, where a much larger part of the predicted crystal landscape was considered and structures with specific properties were targeted (18, 41–44).

Solvates, hydrates and clathrates have previously been the subject of crystal structure prediction studies, although far less often than single-component systems. CSP of multi-component crystals are still rarely attempted because of the difficulty in efficiently sampling the vast space of all possible relative orientations and stoichiometric ratios between the different components, and predictions for multi-component crystals are often less successful than single-component crystals (45).

There are often porous structures in the higher-energy regions of predicted crystal energy landscapes. These usually neglected structures may be empty host frameworks of inclusion compounds, solvates, or clathrates. A few computational studies have explored this possibility, and with notable success. Several such predictions have subsequently been experimentally confirmed (18, 46, 47). Cruz-Cabeza (48) performed CSP on several clathrate forming molecules, including Dianin's compound (49), hydroquinone, *p*-cresol (50), and urea. The calculations successfully reproduced the host structures of several known clathrates, and allowed plausible candidate structures to be proposed for both the *p*-cresol clathrate and the rhombohedral inclusion compound of urea, whose crystal structures had previously not been fully determined (15, 51, 52).

We have previously performed CSP calculations on *o*- and *m*-fluorophenol (CSD: QAMWEH, QAMTUU), in order to determine the crystal structures of their xenon clathrates. By comparing predicted ^{129}Xe shielding tensors with experimentally observed chemical shifts and chemical shift anisotropies, we could propose plausible crystal structures for these clathrates (16–18).

These successful studies show that predictions of clathrate structures in many cases can be effectively accomplished by performing CSP on the host molecule alone, and subsequently inserting guest molecules in predicted porous structures. The method relies on the assumption that the empty host framework is metastable and corresponds to a local lattice energy minimum, which is a reasonable assumption for clathrates with gaseous guests, but probably not for solvates or other multicomponent crystals.

In this article, we present a screening for possible novel clathrates by computational methods. We combine CSP with calculations of the physical properties of a large number of predicted materials in an effort to rationally design functional materials for gas storage and separation.

We describe lattice dynamics (LD) calculations and grand

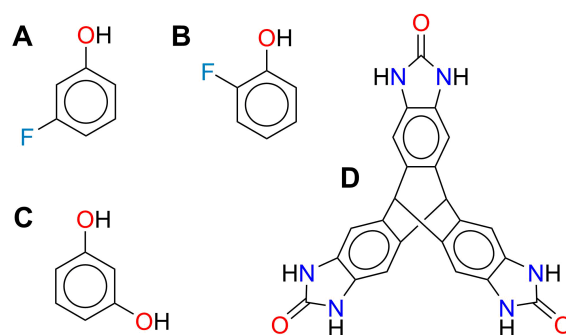


Fig. 1. The clathrate-forming host molecules used in this study. A) *m*-fluorophenol, B) *o*-fluorophenol, C) resorcinol, and D) triptycene trisbenzimidazolone (TTBI). Non-polar hydrogen atoms not shown for clarity.

canonical Monte Carlo (GCMC) simulations on more than 200 hypothetical clathrates. As host molecules, we use *o*- and *m*-fluorophenol, resorcinol (1,3-dihydroxybenzene, CSD: RESORA) and a more complex molecule, triptycene trisbenzimidazolone (TTBI, CSD: DEBXIT), a molecule specifically designed to yield porous crystals, Fig 1 (53, 54). TTBI has four known polymorphs, and all are channel-type inclusion compounds (43).

Resorcinol has three known close-packed polymorphs. It is not known to form clathrates, but based on its similarity to other phenol derivatives and its molecular shape, it is reasonable to speculate that it could form clathrates, and experimental searches have been carried out (55). CSP has previously been performed on resorcinol, using two different methods, in order to elucidate its peculiar helical crystal growth (56). Besides the greenhouse gases CO_2 and CH_4 , we include xenon as one of the guest molecules in this study. Xenon's polarizability makes it bind relatively strongly in clathrates, facilitating their formation, and its chemical shift tensor is extremely sensitive to the atom's immediate surroundings, allowing for precise solid state ^{129}Xe NMR experiments on clathrates. (18, 57).

In summary, we have performed LD and GCMC simulations on more than 200 predicted clathrates of resorcinol, *o*- and *m*-fluorophenol and TTBI with CO_2 , CH_4 and Xe. The study is a wide screening, aiming to identify possible materials suitable for gas separation and storage applications.

Methods

Scope and selection of crystal structures. We have used hypothetical porous crystal structures generated by CSP. The prediction of porous crystal structures of *o*- and *m*-fluorophenol has been reported in a previous article (18). We have also obtained CSP results of resorcinol and TTBI from previous works (47, 58, 59).

From the CSP structure sets we selected plausible clathrate host structures. The structure selection was based on the pore size and dimensionality as calculated with PLATON or (for TTBI) ZEO++ (60, 61). The porosity calculations are performed by placing a probe at every point in a 0.2 Å lattice spanning the unit cell and testing whether the probe is within the van der Waals radius + probe radius (1.2 Å) of any atom

(62–64). For this study, we selected structures with (essentially) discrete pores or narrow channels, see Fig 2.

For the sake of traceability, we keep the original structure names from the CSP studies. Some names originally contained structural information, such as Z' or space group symbols, but here the structure names are arbitrary labels only.

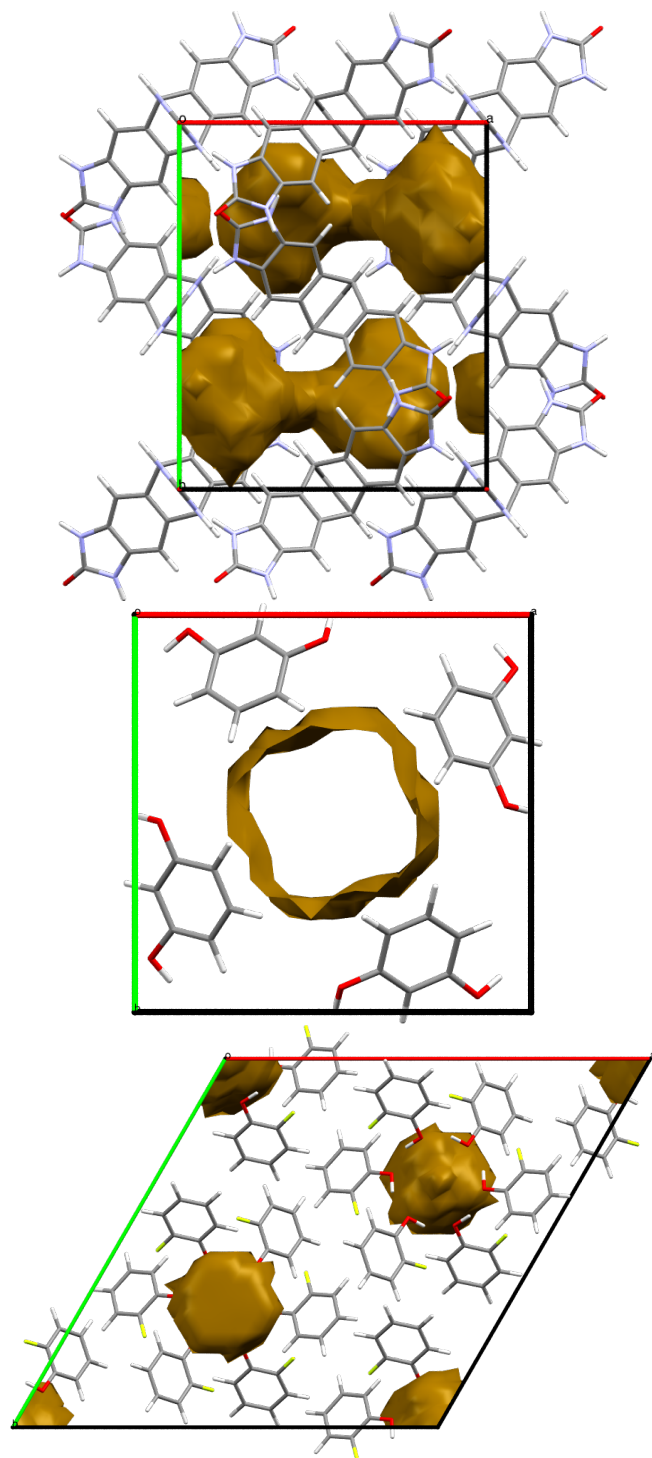


Fig. 2. Crystal packing diagrams of the three example structures. Essentially discrete, but interconnected, pores in the debxit_14_1647 structure of TTBI (top). Typical channel-type cavity in resorcinol_76_3511 (mid), and a β -hydroquinone-like structure of *o*-fluorophenol with completely closed cavities; oF0_R-3_14 (bottom).

In total, 118 porous host structures were considered, but some

were excluded for various reasons. Some could not adsorb any guest molecule without structurally collapsing, some had persistent imaginary phonon frequencies, and some converged to the same structure during geometry-optimization. For example, oF0_1258, oF0_R-3_6 and oF0_R-3_39 all converged to the structure oF00_P-1_14655. Only the latter is included in the final set of results, which contains 84 host structures and their 206 clathrates that appear to be stable and successfully completed all calculations.

The crystal structures studied here, with and without guest molecules, are included in the supplementary information (ESI) as one CIF file containing all 290 crystal structures.

Guest insertion. We have investigated xenon atoms, methane and carbon dioxide as guest molecules. The guest molecules were inserted into crystal structures using a simple docking mechanism. The centre of mass of the guest molecule is placed at the centroid of the cavity, as determined with PLATON. For guests other than xenon, the molecule was then rotated randomly until there were no clashes between atoms, using 85% of the summed van der Waals radii as the criterion for a clash. Guest insertion was performed into the crystal structures in space group $P1$, so that we did not restrict the positions and orientations of the guest to the symmetry of the original host structure. The guest docking was repeated until there were no more empty cavities in the unit cell. The structures were then relaxed by energy minimization, see below.

The carbon dioxide molecules were supplemented with four non-interacting dummy atoms located around the carbon atom, since the program DMACRYS cannot handle linear molecules (65).

The packing coefficient of the guest was calculated from the solvent-accessible void volumes, as calculated with PLATON, and the molecular van der Waals volumes: 25.85 Å³ for CH₄, 38.16 Å³ for CO₂ and 42.21 Å³ for Xe.

Energy model. Several of the methods and programs used have been described in detail elsewhere (27, 65, 66). The intermolecular (lattice) energy E_{latt} is calculated with an atom-atom force field that includes electrostatic interactions between distributed multipoles derived from the molecule's charge density, as calculated with PBE0/6-311G(d,p). A polarizable continuum model (PCM) (67) with a relative permittivity of $\epsilon = 5.0$ was used to model the polarization of the molecule in the crystal. All DFT calculations were performed with the GAUSSIAN 09 program (68).

Intermolecular interactions between each pair of molecules M and N were modelled with an anisotropic force field of the *exp-6* form, and with distributed electrostatic multipoles:

$$E_{\text{inter}}^{MN} = \sum_{i,k} \left(A^{\iota\kappa} \exp(-B^{\iota\kappa} R_{ik}) - C^{\iota\kappa} R_{ik}^{-6} + E_{ik}^{\text{DMA}} \right) \quad (1)$$

where i and k are atoms of type ι and κ belonging to molecules M and N respectively, separated by the distance R_{ik} . The dispersion-repulsion force field parameters $A^{\iota\kappa}$, $B^{\iota\kappa}$ and $C^{\iota\kappa}$ were taken from the W99rev6311P force field

(26, 66), supplemented with parameters for xenon (18). As is always done with the Williams force fields, the bond lengths to hydrogen atoms were shortened by 0.1 Å (69, 70). Electrostatic multipoles were calculated from the molecular charge densities with the GDMA program by Anthony Stone (71). Multipoles up to rank 4 (hexadecapoles) were distributed onto all atoms. Ewald summation was used for charge-charge, charge-dipole and dipole-dipole interactions, while dispersion-repulsion and interactions between higher multipoles were summed between whole molecules up to a centre of mass distance of 15 Å.

By E_{latt} we mean the sum of all intermolecular interactions per mole host molecule. The total energy of a whole simulation supercell with Z host molecules is ZE_{latt} .

Lattice dynamics. Phonon frequencies are useful to us for three reasons. First, that all frequencies are real confirms that the structure corresponds to an energy minimum. Secondly, they allow us to calculate the vibrational entropic contribution to the binding energy of the guests. And finally, phonon frequencies can be compared to experimental Terahertz or low-frequency Raman spectra, possibly allowing structural determination by direct comparison to predicted frequencies (72, 73).

Rigid-molecule geometry optimizations and lattice dynamics calculations, using the above force field, were performed with DMACRYS (65, 74).

The total number of non-zero phonons is $n = 6ZN_{\text{k}} + N_{\text{d}}N_{\text{g}}N_{\text{k}} - 3$, N_{k} is the number of sampled \mathbf{k} -points, N_{d} , the number of degrees of freedom for the guest molecule (3 for Xe, 5 for CO₂ and 6 for CH₄), and N_{g} the number of guest molecules per simulation cell.

The main difficulty in lattice dynamics lies in the poor convergence of the vibrational energy with respect to Brillouin zone sampling. We performed simulations on supercells, the dimensions of which were determined from the requirement that the reciprocal lattice vectors of the empty host structure were all smaller than $2\pi \times 0.07 \text{ \AA}^{-1}$. In addition, we used Debye's method to model phonon dispersion of the three acoustic modes, as described elsewhere (27, 75). A linear phonon dispersion can be assumed for the acoustic modes near the Γ -point and the dispersion relation is determined from the elastic tensor and the Christoffel equation.

Phonon dispersion around other \mathbf{k} -points was modelled as a kernel density estimate (KDE) (76). We and others have previously used Gaussian kernel density estimates for this purpose (66, 77). However, invoking Debye's assumption of a linear phonon dispersion within a small sphere around each \mathbf{k} -point (78), it can be shown that the dispersion can be effectively modelled by substituting each discrete phonon frequency ω_i with an Epanechnikov kernel function (79);

$$K(x) = \frac{3}{4}(1-x^2)\text{I}(x) \quad (2)$$

where $\text{I}(x)$ denotes the indicator function

$$\text{I}(x) = \begin{cases} 0, & \text{if } |x| \geq 1 \\ 1, & \text{if } |x| < 1 \end{cases} \quad (3)$$

The phonon density of states of the non-zero optical phonons ω_i is then:

$$g_{\text{O}}(\omega) = \frac{3}{4bN_{\text{k}}} \sum_i^n \left(1 - \left(\frac{\omega - \omega_i}{b} \right)^2 \right) \text{I} \left(\frac{\omega - \omega_i}{b} \right) \quad (4)$$

We have explored the possibility of automatically choosing the kernel bandwidth b by means of least-squares cross-validation, or from finite differences in phonon frequencies between \mathbf{k} -points (80, 81), but this proved highly impractical (76, 79). Instead, we have set $b = 6 \text{ cm}^{-1}$, which, based on experience, seems reasonable.

According to Debye's approximation, the density of states of the 3 acoustic modes is:

$$g_{\text{A}}(\omega) = \frac{9}{N_{\text{k}}\omega_{\text{D}}^3} \omega^2, \quad 0 < \omega < \omega_{\text{D}} \quad (5)$$

where ω_{D} is the Debye frequency, which we obtain from the elastic stiffness tensor, as described elsewhere (66, 75). The total density of states $g(\omega)$ is $g_{\text{O}}(\omega) + g_{\text{A}}(\omega)$.

The vibrational energy per mole of host molecule is calculated as:

$$F_{\text{vib}}(T) = \frac{1}{4Z\pi} \int_0^\infty h\omega g(\omega) d\omega + \frac{k_{\text{B}}T}{Z} \int_0^\infty g(\omega) \ln \left(1 - \exp \left(\frac{-h\omega}{2\pi k_{\text{B}}T} \right) \right) d\omega \quad (6)$$

The integrals were evaluated numerically with Romberg's method. In a couple of cases, they did not converge, and we then reverted to using a Gaussian KDE with half the bandwidth, which gives virtually identical results (40).

The adsorption energies are calculated as the static E_{latt} and vibrational energies F_{vib} of the fully saturated clathrate relative to that of the empty host framework and the ideal gas at 300 K and 1 bar:

$$\Delta E_{\text{latt}}^{\text{bind}} = \frac{Z}{N_{\text{g}}} \left(E_{\text{latt}}^{\text{clathrate}} - E_{\text{latt}}^{\text{host}} \right) \quad (7)$$

$$\Delta F_{\text{vib}}^{\text{bind}} = \frac{Z}{N_{\text{g}}} \left(F_{\text{vib}}^{\text{clathrate}} - F_{\text{vib}}^{\text{host}} \right) - \mu \quad (8)$$

where μ is the chemical potential of the ideal gas, see Equations 11 – 13 below.

Monte Carlo simulations. A grand canonical (constant μ VT) Monte Carlo simulation method was implemented in order to determine the equilibrium gas adsorption at different pressures and temperatures. The method, based on Frenkel and Smit (82), was written in Python. The host molecules were held fixed, and only the guest molecules were subject to Monte Carlo moves. Insertions, deletions and translations were equally likely to be attempted. Translations and insertions were always performed after the molecule had been randomly rotated. Insertions and translations were attempted at randomly chosen positions independent of the molecule's previous position. Pseudo-random numbers were used, and

uniformly distributed rotation matrices were generated with Arvo's fast method (83).

Simulations were performed on supercells created by elongating the single shortest lattice vector until the supercell contained 16 molecules of TTBI or 18 molecules of the other compounds. The program DMACRYS and the multipole-based force field described above were used to calculate the energy of the Monte Carlo configurations. However, for computational speed and convenience, it is necessary to identify and reject simulation frames containing atom clashes, *i.e.* where atoms are unrealistically close to each other. This is formally equivalent to including a hard-sphere potential term E^{HS} to the sum in Equation (3), with the form:

$$E_{ik}^{\text{HS}} = \begin{cases} \infty, & R_{ik} < R_i^{\text{vdW}} + R_k^{\text{vdW}} - 0.7 \text{ \AA} \\ 0, & \text{otherwise} \end{cases} \quad (9)$$

where R^{vdW} denote the CSD-average van der Waals radius of the atom (84).

The gases were treated as ideal. The thermal de Broglie wavelength for an ideal gas is

$$\Lambda = \frac{h}{\sqrt{2\pi m k_B T}} \quad (10)$$

where m is the molecular mass. For carbon dioxide and methane, we include the chemical potential from the rotational degrees of freedom μ^{rot} , obtained as:

$$\mu_{\text{CO}_2}^{\text{rot}} = -k_B T \ln \left(\frac{8\pi^2 I k_B T}{\sigma h^2} \right) \quad (11)$$

$$\mu_{\text{CH}_4}^{\text{rot}} = -k_B T \ln \left(\frac{8\pi^2 (2\pi I k_B T)^{3/2}}{\sigma h^3} \right) \quad (12)$$

where I is the moment of inertia and σ a symmetry number, 2 for CO_2 and 12 for CH_4 . The chemical potential is then

$$\mu = \mu^{\text{rot}} + k_B T \ln \left(\frac{\Lambda^3 P}{k_B T} \right) \quad (13)$$

Monte Carlo moves involving translations and rotations are accepted with the usual Metropolis criterion. Particle insertions (+) and deletions (-) are accepted with a probability calculated as:

$$P(+)=\min\left(1,\frac{V}{\Lambda^3(N_g+1)}\exp\left(\frac{\mu-Z\Delta E_{\text{latt}}}{k_B T}\right)\right) \quad (14)$$

$$P(-)=\min\left(1,\frac{\Lambda^3 N_g}{V}\exp\left(\frac{-\mu-Z\Delta E_{\text{latt}}}{k_B T}\right)\right) \quad (15)$$

Simulations were performed on all 206 stable clathrate structures, at 9 temperatures between 200 and 400 K and for 6 pressures between 0.05 and 4 bar, *i.e.* more than 11.000 Monte Carlo simulations. These simulations were executed on an in-house computer cluster, using an *ad hoc* Python server-client implementation based on CLilly (85). The GCMC simulations required about 90.000 CPU-hours, all

other calculations performed in this study are negligible in comparison.

Each simulation was run until 2000 energy-evaluations had been performed, and every tenth such configuration was saved and used for ensemble averaging. The relatively small number of energy-evaluations are due to the vast majority of Monte Carlo iterations being discarded due to hard-sphere overlaps and without energy-evaluation.

The heat of desorption q (per mole gas) was calculated from ensemble averages as (86):

$$q = \frac{\langle N_g Z E_{\text{latt}} \rangle - \langle Z E_{\text{latt}} \rangle \langle N_g \rangle}{\langle N_g^2 \rangle - \langle N_g \rangle^2} \quad (16)$$

This estimate depends on an adequate sampling over a range of guest occupations, and should be most reliable for those clathrates where the simulation covered both fully saturated and completely empty structures. The heat of desorption does not vary substantially with temperature or pressure, why we report the average across all simulated temperatures and pressures \bar{q} . The experimentally observable isosteric heat of adsorption is $-\bar{q} + RT$.

Our multipole-based force field for intermolecular interactions should be highly reliable, and has performed very well in the past (40). Some approximations are however necessary to be able to carry out a screening of so many structures. We have re-optimized the crystal structures after guest insertion, so the calculated lattice energies and lattice dynamics simulations do account for the relaxation of the host structure around the guest. However, this effect is not included in the grand canonical Monte Carlo simulations. The host structure is held fixed, and while this is computationally convenient, it neglects the fact that the host molecules also have thermal motion and that the unit cell expands and contracts with respect to temperature, pressure and the presence of guest molecules. Such effects are however not expected to greatly influence the results, since organic molecular crystals generally change in volume and lattice parameters by a mere 3% to 5% over the pressure- and temperature ranges we explore here (66). The changes in unit cell volumes in response to guest occupation are about as large (79).

Results

Binding energies and lattice dynamics. We present results on general trends over all clathrates and detailed results for three representative examples, namely the structures shown in Fig 2. Most results are presented in the supplementary information, and include packing diagrams, phonon spectra and adsorption isotherms for all structures.

The three example crystal structures have different kinds of pores. The resorcinol structure resorcinol_76_3511 is a channel-type inclusion compound; the four-fold screw axis of space group $P4_1$ results in the formation of open channels. The *o*-fluorophenol structure oF0_R-3_14 has the hexagonal $R\bar{3}$ -motif common to all known clathrates of the phenol-type. Most predicted host structures of the fluorophenols have this symmetry. The TTBI structure debxit_14_1647

belongs to $P2_12_12$, ($P2_111$ if intramolecular symmetry is ignored). The cavities are interconnected by narrow bottlenecks, possibly facilitating gas diffusion through the crystal structure.

Molecular crystals are almost always close-packed with packing coefficients near 70% (87). In real clathrates, and in most of our predicted structures, the guest molecules have a significantly looser packing. However, the cavity volume calculation is imprecise, and guest packing coefficients are in some cases not well-defined. In channels or extended networks of interconnected pores, it is not possible to calculate a packing coefficient for the guest. We have therefore plotted results in Fig. 3–4 only for the majority of structures with well-defined guest packing coefficient, see the ESI for details.

The distribution of guest packing coefficients is centered near 55%, but has a wider range than expected. That is, some apparently stable structures have cavities that seem too small or too large for its guest. Many of the structures however appear to have near ideal cavities for CO_2 and Xe.

In Fig 3 (top), we see that, contrary to expectation, there is no correlation between the static (0 K) binding energies and the cavity size. It is surprising to see that strong binding ($E_{\text{latt}}^{\text{bind}} < -35$ kJ/mol) can occur with packing coefficients as small as 25% and as large as 80%.

Methane is generally less strongly bound than CO_2 and Xe. Methane is however not as strongly penalized by the loss of entropy as CO_2 , presumably because methane molecules are quite free to rotate in the clathrates, which carbon dioxide, being a linear molecule cannot.

The two structures that bind CO_2 the strongest are oF0_R-3_17 and oF0_R-3_20, these both belong to the class of hexagonal $R\bar{3}$ -symmetric structures that strongly resemble hydroquinone clathrates, see also the very similar *o*-fluorophenol structure in Fig 2. These two structures bind CO_2 with a heat of desorption of -60 kJ/mol and -52 kJ/mol, respectively, which can be compared to the isosteric enthalpy of adsorption of CO_2 on active charcoal which is typically between 15 and 25 kJ/mol (88, 89), nanoporous carbon 16 to 33 kJ/mol (90), and amine-functionalized mesoporous silicas 65–78 kJ/mol (91).

The guest molecules introduce new lattice vibrational modes in the crystals, which give the clathrates a stabilizing contribution to the free energy. In Fig 3 (middle) we show the spread in $F_{\text{vib}}^{\text{bind}}$ calculated at 300 K. Again, there is a wide range, and no apparent correlation with respect to the packing coefficient of the guest molecules.

The heat of desorption \bar{q} takes the anharmonic thermal motion of the guest into account and should be a good estimate of the experimental isosteric heat of adsorption. It is calculated as an average over all simulations at all temperatures and pressures for each clathrate. The results are shown in the bottom panel of Fig 3.

We can compare the heats of desorption calculated from static (0 K) lattice energies with the more realistic estimate \bar{q} from the grand canonical ensembles, see Fig 4. There is a correlation, as expected, but it is weak. Hence, using only lattice energies to assess the affinity of gases in clathrates at

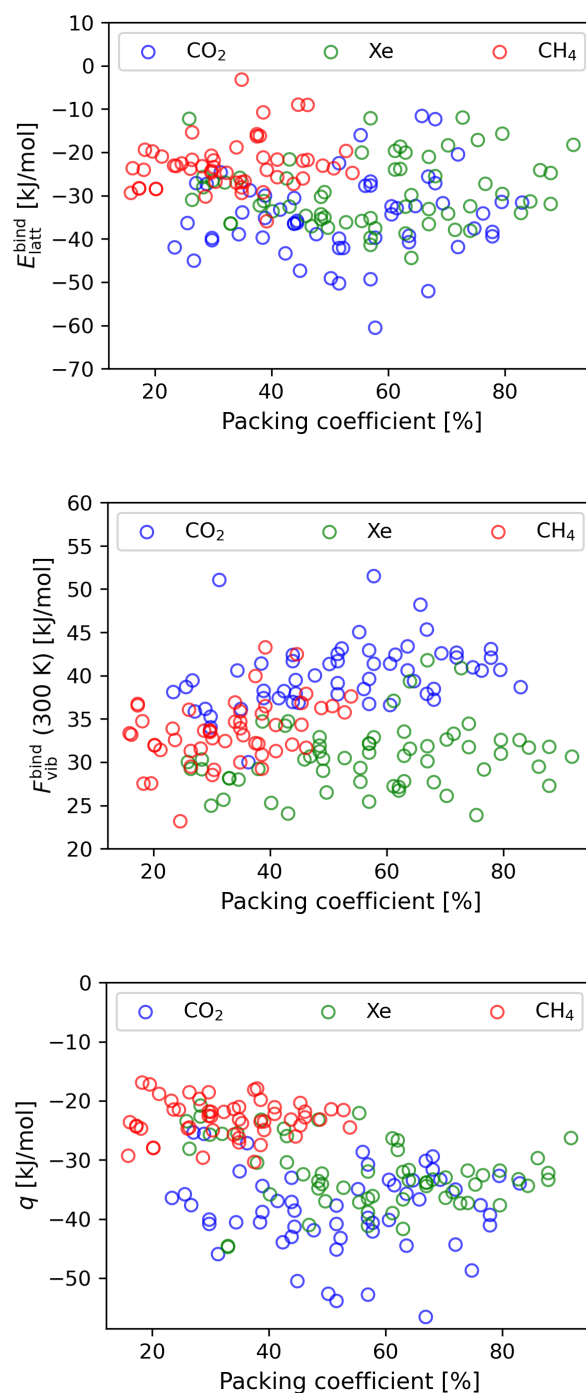


Fig. 3. (top) The lattice energy stabilization of CH_4 clathrates are typically 10–30 kJ/mol, and 20–50 kJ/mol for CO_2 and Xe, relative to the empty host structure. There is no correlation between the static binding energy $E_{\text{latt}}^{\text{bind}}$ and the size of the cavity. (middle) The vibrational contribution to the free energy is also independent of the cavity size. (bottom) The ensemble-average heat of desorption q ranges approximately from -15 to -30 kJ/mol for CH_4 and -20 to -50 kJ/mol for the other gases. Again, there is no correlation between the adsorption energy q and the size of the cavity.

finite temperature is unlikely to give reliable results.

The binding energies, in the form of the static (lattice) energy contribution $E_{\text{latt}}^{\text{bind}}$, the guest’s contribution to the vibrational energy $F_{\text{vib}}^{\text{bind}}$, and the ensemble-averaged heat of adsorption q for the different clathrates are shown in Tab 1. The vibra-

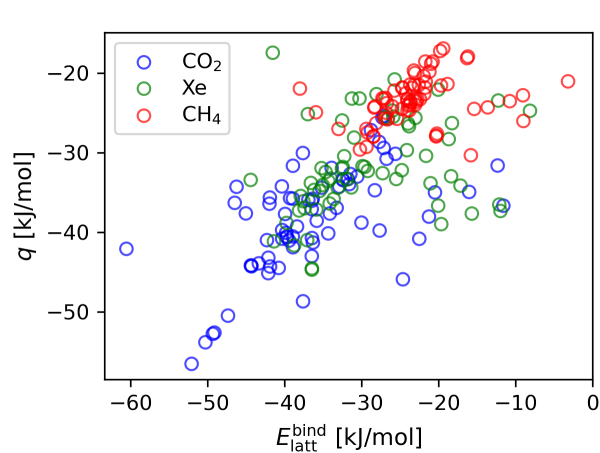


Fig. 4. The static (0 K) desorption energy is weakly correlated with the ensemble-average desorption energy q .

tional energy depends on temperature and pressure and was evaluated at 300 K and 1 bar.

Clathrate	$E_{\text{latt}}^{\text{bind}}$	$F_{\text{vib}}^{\text{bind}}$	\bar{q}
debxit_14_1647_CH4	-28.5	31.9	-28.0
debxit_14_1647_CO2	-39.8	34.0	-40.1
debxit_14_1647_Xe	-36.5	28.1	-44.6
resorcinol_76_3511_CH4	-19.8	27.5	-17.2
resorcinol_76_3511_CO2	-27.3	36.2	-25.6
resorcinol_76_3511_Xe	-27.0	25.7	-25.6
oF0_R-3_14_CH4	-23.4	28.5	-21.9
oF0_R-3_14_CO2	-36.3	39.5	-41.3
oF0_R-3_14_Xe	-35.1	29.0	-34.1

Table 1. Adsorption energies, in kJ/mol, for some representative clathrates. The vibrational energy is a function of temperature and pressure and was calculated for 300 K and 1 bar.

Phonon densities of states for the structures debxit_14_1647, resorcinol_76_3511, oF180_R-3_51, and their fully occupied clathrate structures are shown in Fig 5. Guest inclusion typically modifies some of the host's phonon modes and leaves other modes unaffected. Methane often introduced new distinct high-frequency vibrations, while xenon introduces low-frequency modes. Note the Debye approximation that leads to a small interval at very low frequencies where the DOS depends quadratically on the frequency, as per Eq. 5.

GCMC results. Thanks to the hard-sphere potential and the immediate rejection of unphysical configurations, equilibration and convergence are reached relatively quickly. The convergence is plotted for three examples where the clathrates are about 2/3 full, see Fig 6. Only Monte Carlo moves that did not result in a hard-sphere clash were energy-evaluated, and only those iterations are shown in the figure. For each such iteration, there were on the order of 100 Monte Carlo moves that were not counted. Hence, the true number of Monte Carlo moves in each simulation was around 200,000. However, the adsorption isotherms show artifacts due to non-convergence, the guest adsorption does not always depend

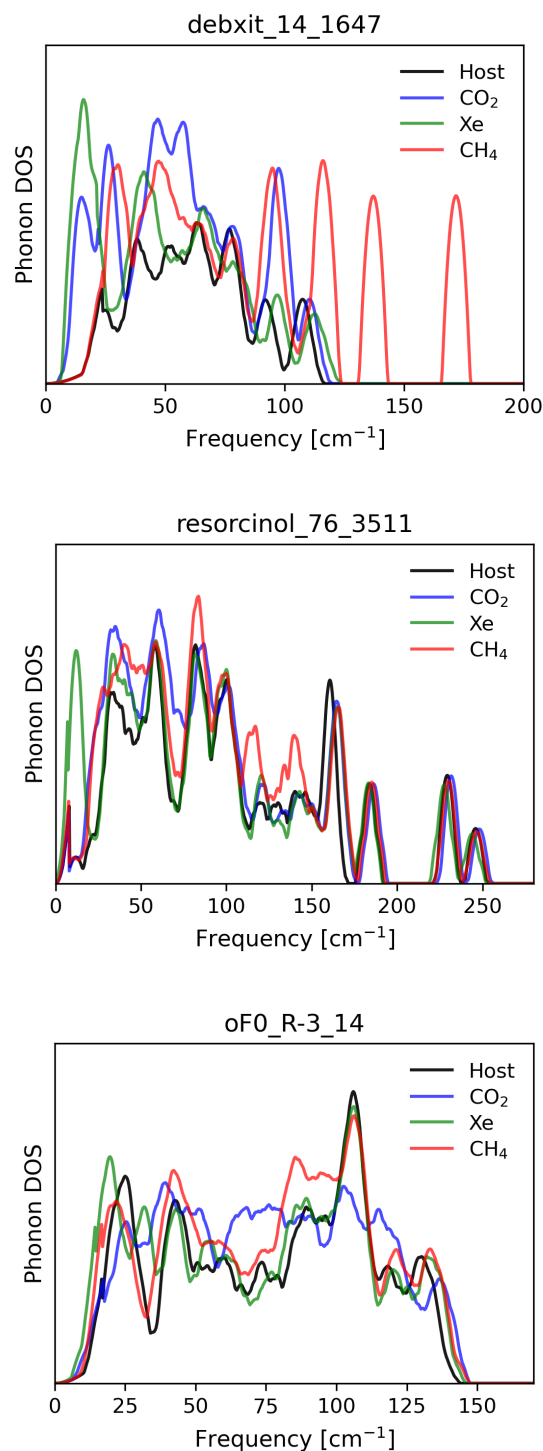


Fig. 5. Phonon densities of states for the structures debxit_14_1647, resorcinol_76_3511, oF0_R-3_14, and their fully occupied clathrate structures.

monotonically on temperature and pressure. Hence, for quantitative calculations of the properties of clathrates, we recommend simulations that are longer than those used here for screening a large number of structures.

We have calculated the equilibrium adsorption for all clathrates at 6 pressures and 7 temperatures between 200 K and 350 K. For the examples presented here, we have extended the temperature range to 400 K to better show the

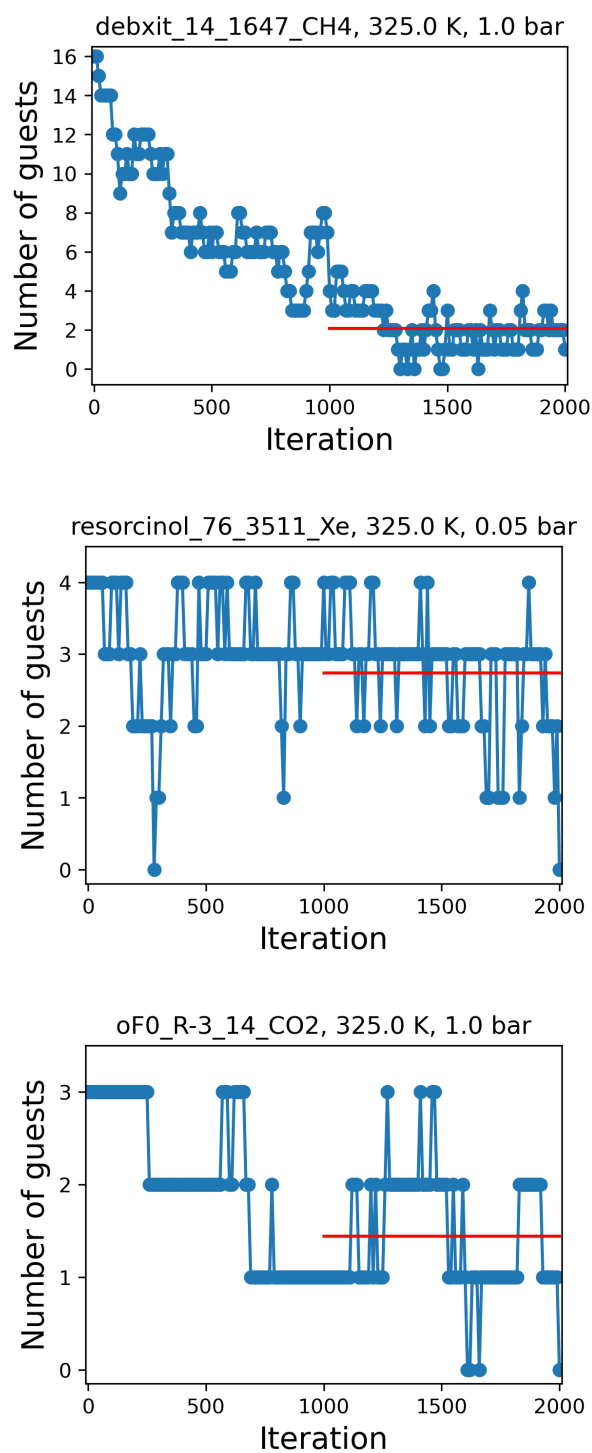


Fig. 6. Example convergences of grand canonical Monte Carlo simulations. Only iterations where energy-evaluations were performed are counted. The first half of the simulation was used for equilibration, ensemble averages were calculated over the 1000 last iterations (red line). Green lines are 11-iterations moving averages.

desorption, especially of Xe, which tends to adsorb strongly even above room temperature.

A. Results for example structures. The results are shown in Figs. 7–9. The white dots show the pressure and temperature combinations where Monte Carlo simulations were per-

formed, the stoichiometry between the dots is interpolated by a piecewise cubic polynomial. For debxit_14_1647, we see that the structure is completely saturated with Xe (1:1 TTBI:Xe stoichiometry) at all temperatures and pressures, with only a hint of desorption at 400 K and 0.05 bar. Many of the structures in our study bind xenon that strongly. The other gases however are generally less strongly bound.

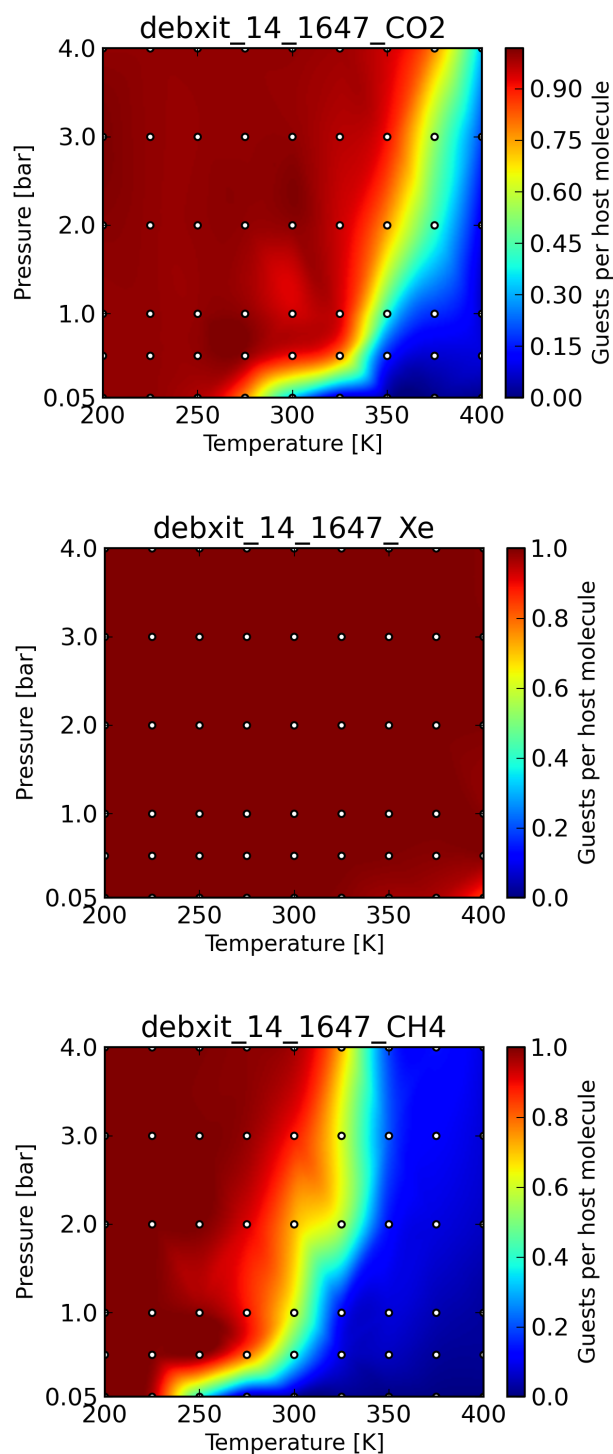


Fig. 7. Adsorption isotherms for clathrates of debxit_14_1647. Monte Carlo Simulations were performed at temperature and pressure combinations marked by white dots. The areas between the dots are interpolated.

We note that the adsorption isotherms are generally not strictly monotonic, which is an artefact that arises because the calculations are not completely converged. Longer Monte Carlo simulations are probably needed to obtain reliable quantitative estimates for the gas adsorption, but to completely converge all 10,000 simulations would be prohibitively costly and beyond the scope of this initial screening.

The adsorption of gases in the resorcinol_76_3511 structure is presented in Fig. 8. Note the scale, the maximum value (dark red) is for a completely saturated structure (4:1 host-guest stoichiometry in this case). This resorcinol structure also binds xenon the strongest, and both CH₄ and CO₂ are quite poorly adsorbed at all pressures and temperatures above 200 K. Again, this is representative of many of the clathrates in this study.

In Fig 9 we see the adsorption behaviour of the hydroquinone-type oF0_R-3_14 structure. This structure adsorbs CO₂ strongly even at room temperature and 1 bar of CO₂ pressure, in addition, the adsorption at 1 bar is strongly temperature-dependent around 300 K, possibly facilitating reversible adsorption by temperature regulation. This structure also has a large difference in affinity for CO₂ and CH₄, properties which may make it suitable for CO₂ scrubbing from flue gases or for upgrading biogas, assuming the predicted structure can be realized.

Conclusions

Powell pointed out, in 1950, that it is impossible to make reliable predictions as to which substances will form a clathrate structure (92). This is no longer true. Crystal structure prediction in combination with grand canonical Monte Carlo simulations is a powerful method for the prediction of clathrate structures and their properties. Using such methods and a highly accurate multipole-based force field, we have predicted novel clathrates of resorcinol, *o*- and *m*-fluorophenol and TTBI that adsorb CO₂, CH₄ and Xe. We have found 84 structures that are mechanically stable both when empty and fully saturated with guest molecules. We have calculated the equilibrium adsorption of Xe, CH₄ and CO₂, at several temperature and pressures, finding that Xe is in general most strongly adsorbed, and CH₄ quite weakly. Several structures are fully occupied with xenon even at room temperature and pressure, suggesting they may form quite easily. We have also found structures that adsorb CO₂, for instance mF180_R-R_18, see Fig 10. This structure, which has an unusually large CO₂ heat of desorption, $q = -52.8$ kJ/mol, adsorbs large quantities of CO₂ even below 1 bar of CO₂ pressure and above room temperature. The cavity to guest volume ratio for this structure is ideal, 57%.

Our results suggest that, just like a molecule can have several polymorphs, there may be several clathrates of a given molecule, for TTBI, a molecule designed to form porous crystals, this is already known to be true.

Because of the commercial incentives, CSP is mostly used on novel pharmaceuticals, where the goal is to identify the thermodynamically stable form for development into a drug

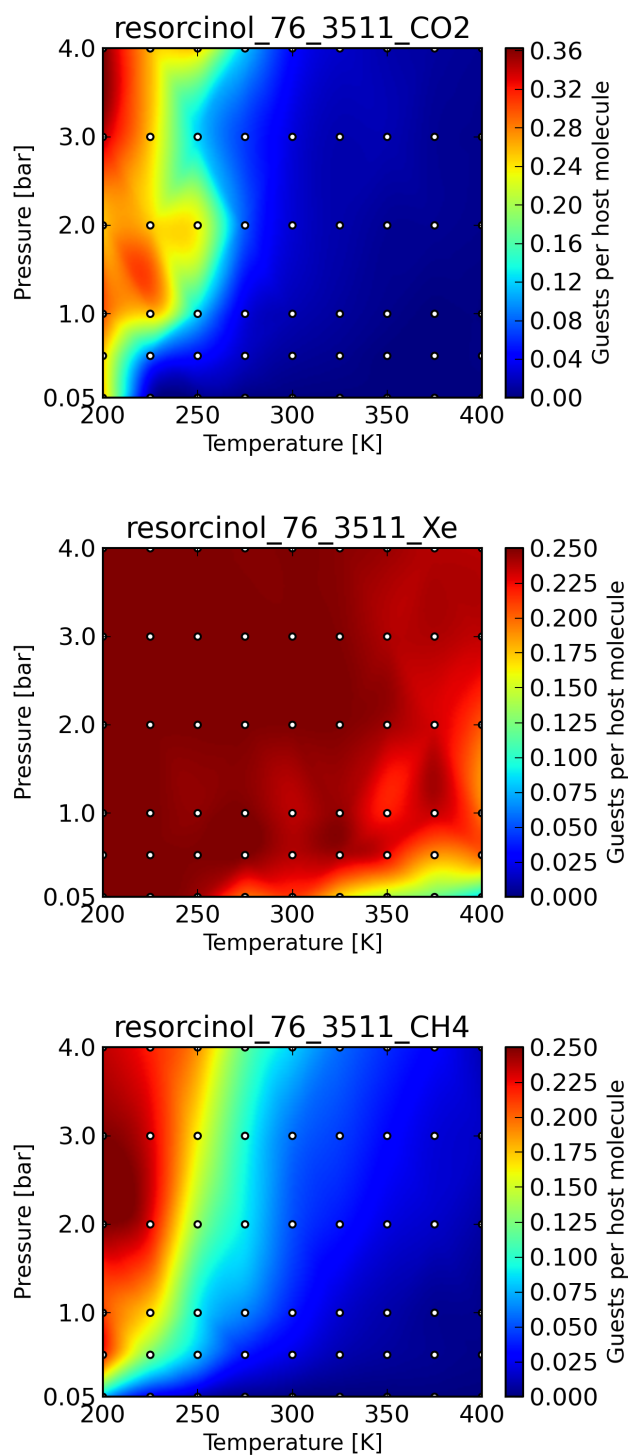


Fig. 8. Adsorption isotherms for clathrates of resorcinol_76_3511.

product (85). As demonstrated here, CSP is useful also for other purposes, especially in the search for, and rational design of, functional materials. In particular, unstable or exotic materials that are challenging to study experimentally at ambient conditions on Earth are particularly suitable for computational modelling (93, 94).

The predicted clathrate structures are included as CIF files in the supplementary information. They should be valuable

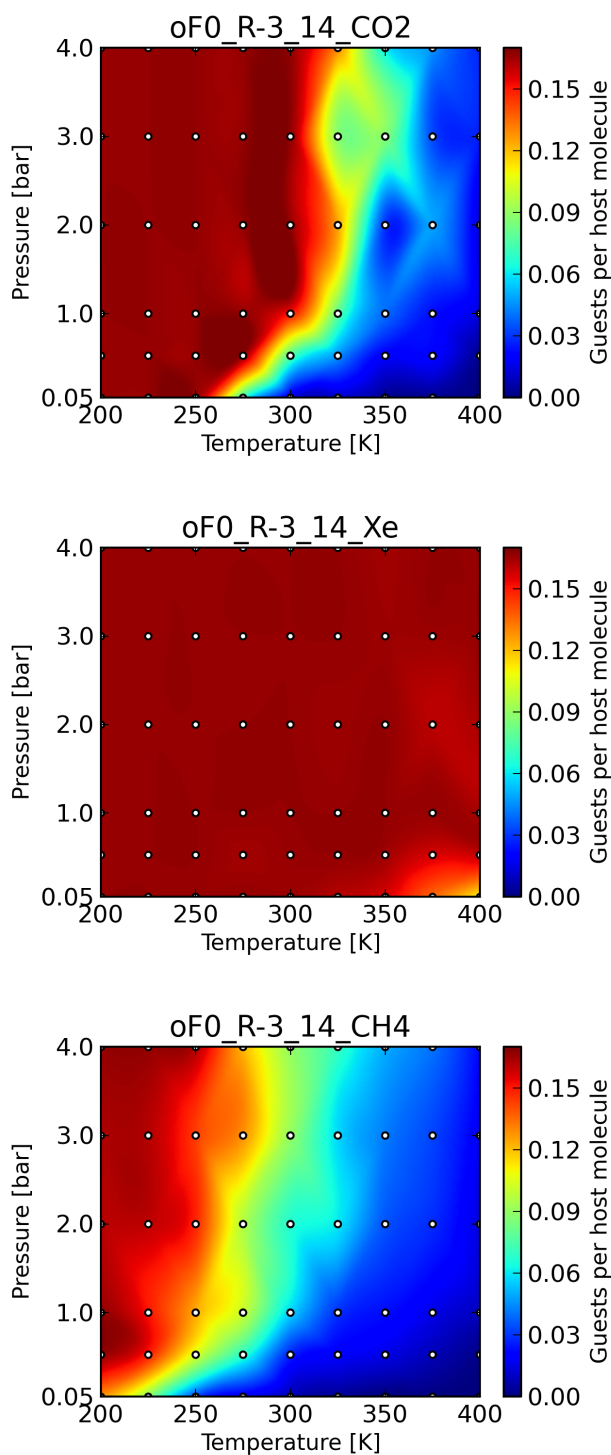


Fig. 9. Adsorption isotherms for clathrates of oF0_R-3_14.

when experimentally searching for new clathrates of these compounds, since simulated powder X-ray diffraction patterns, NMR-, Raman- and THz-spectra of these structures may allow identification of new phases by direct comparison between simulated and experimental data (18, 72, 73, 95, 96). The adsorption of gases in clathrates depends on both enthalpic and entropic contributions. We calculated the static temperature-free adsorption energy, a vibrational energy, as

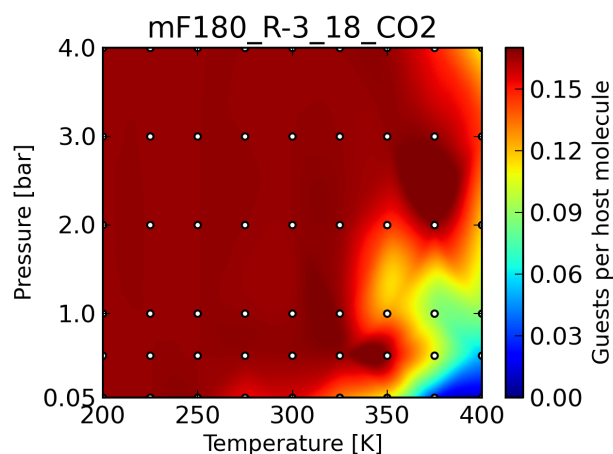


Fig. 10. Adsorption isotherms for the *m*-fluorophenol structure mF180_R-3_18. This structure is predicted to adsorb CO₂ even at above room temperature and at reduced pressures.

well as an ensemble-average heat of adsorption. We expected to find dependencies between these quantities and the size of the cavities. Naïvely, one would expect that small pores are enthalpically favoured, while larger pores allow the guests to move more freely, contributing additional entropy. Surprisingly, we found that apparently (meta-)stable structures that are able to adsorb quantitatively can have a very wide range of packing coefficients, and that there are no apparent correlations between cavity size and thermodynamics.

Perhaps needless to say, we encourage the scientific community to try to isolate the predicted clathrates.

ACKNOWLEDGEMENTS

We thank Peter J. Bygrave and Angeles Pulido for providing previously predicted crystal structures of resorcinol and TTBI, respectively. We thank Mariia Bilinska for translating ref. 16 from Russian. The research leading to these results has received funding from the Swedish Energy Agency grant 49215-1.

COMPETING FINANCIAL INTERESTS

All three authors declare that we have no competing interests.

Bibliography

1. H. M. Powell. The structure of molecular compounds. Part IV. Clathrate compounds. *J. Chem. Soc.*, pages 61–73, 1948.
2. L. Mandelcorn. Clathrates. *Chem. Rev.*, 59(5):827–839, 1959.
3. Yu A. Dyadin, I. S. Terekhova, T. V. Rodionova, and D. V. Soldatov. Half-century history of clathrate chemistry. *J. Struct. Chem.*, 40(5):645–653, 1999.
4. A. I. Kitaigorodsky. *Molecular Crystals and Molecules*. Physical Chemistry. Academic Press, Inc, 1973.
5. A. Burger and R. Ramberger. On the polymorphism of pharmaceuticals and other molecular crystals. I. *Microchim. Acta*, 72(3-4):259–271, 1979.
6. D. D. MacNicol, J. J. McKendrick, and D. R. Wilson. Clathrates and molecular inclusion phenomena. *Chem. Soc. Rev.*, 7(1):65–87, 1978.
7. Steven C Zimmerman. Putting molecules behind bars. *Science*, 276(5312):543–544, 1997.
8. DE Palin and HM Powell. The structure of molecular compounds. part vi. the β -type clathrate compounds of quinol. *Journal of the Chemical Society (Resumed)*, pages 815–821, 1948.
9. J.-P. Torré, R. Coupan, M. Chabod, E. Pere, S. Labat, A. Khoukh, R. Brown, J.-M. Sotiropoulos, and H. Gornitzka. CO₂-hydroquinone clathrate: Synthesis, purification, characterization and crystal structure. *Cryst. Growth Des.*, 16(9):5330–5338, 2016. doi: 10.1021/acs.cgd.6b00834.
10. J. L. Daschbach, T.-M. Chang, L. R. Corrales, L. X. Dang, and P. McGrail. Molecular mechanisms of hydrogen-loaded β -hydroquinone clathrate. *The Journal of Physical Chemistry B*, 110(35):17291–17295, 2006.
11. K. W. Han, Y.-J. Lee, J. S. Jang, T.-I. Jeon, J. Park, T. Kawamura, Y. Yamamoto, T. Sugahara, T. Vogt, and J.-W. *et al.* Lee. Fast and reversible hydrogen storage in channel cages of hydroquinone clathrate. *Chem. Phys. Lett.*, 546:120–124, 2012.
12. V. F. Rozsa and T. A. Strobel. Triple guest occupancy and negative compressibility in hydrogen-loaded β -hydroquinone clathrate. *J. Phys. Chem. Lett.*, 5(11):1880–1884, 2014.

13. J.-W. Lee, S.-P. Kang, and J.-H. Yoon. Competing occupation of guest molecules in hydroquinone clathrates formed from binary C₂H₄ and CH₄ gas mixtures. *The Journal of Physical Chemistry C*, 118(14):7705–7709, 2014.
14. J.-W. Lee, P. Dotel, J. Park, and J.-H. Yoon. Separation of CO₂ from flue gases using hydroquinone clathrate compounds. *Korean Journal of Chemical Engineering*, 32(12):2507–2511, 2015.
15. R. M. Barrer and V. H. Shanson. Clathration by para-substituted phenols. *J. Chem. Soc. Faraday Trans.*, 72:2348–2354, 1976.
16. Yu. N. Kazankin, A. A. Palladiev, and A. M. Trofimov. Clathrate compound of meta-fluorophenol with xenon. *Zh. Obshch. Khim.*, 41(11):2268–2370, 1972. in Russian.
17. Yu. N. Kazankin, A. A. Palladiev, and A. M. Trofimov. Clathrate compound of ortho-fluorophenol with xenon. *Zh. Obshch. Khim.*, 43(12):2670–2671, 1973. in Russian.
18. Marcin Selent, Jonas Nyman, Juho Roukala, Marek Ilczyszyn, Rajja Oilunkaniemi, Peter J Bygrave, Risto Laitinen, Jukka Jokisaari, Graeme M Day, and Perttu Lantto. Clathrate structure determination by combining crystal structure prediction with computational and experimental 129Xe nmr spectroscopy. *Chemistry—A European Journal*, 23(22):5258–5269, 2017.
19. Peter Englezos. Clathrate hydrates. *Industrial & engineering chemistry research*, 32(7):1251–1274, 1993.
20. Jiyeon Lim, Wonjung Choi, Junghoon Mok, and Yongwon Seo. Clathrate-based CO₂ capture from CO₂-rich natural gas and biogas. *ACS Sustainable Chemistry & Engineering*, 6(4):5627–5635, 2018.
21. V. E. Zubkus, I. L. Shamovsky, and E. E. Tornau. Computer-simulation studies of β -quinol clathrate with various gases. Molecular interactions and crystal structure. *J. Chem. Phys.*, 97(11):8617–8627, 1992.
22. K. Hermansson. Host-guest interactions in an organic crystal: β -hydroquinone clathrate with Ne and HF guests. *The Journal of Chemical Physics*, 112(2):835–840, 2000.
23. A. Nemkevich, M. A. Spackman, and B. Corry. Simulations of guest transport in clathrates of Dianin's compound and hydroquinone. *Chem. Eur. J.*, 19(8):2676–2684, 2013.
24. A. Nemkevich, M. A. Spackman, and B. Corry. Mechanism of concerted hydrogen bond reorientation in clathrates of Dianin's compound and hydroquinone. *Journal of the American Chemical Society*, 133(46):18880–18888, 2011. doi: 10.1021/ja206962f. PMID: 21988055.
25. P. Dansas and P. Sixou. Liberté de reorientation et mise en ordre cooperative dans les clathrates d'hydroquinone. *Molecular Physics*, 31(5):1297–1318, 1976. doi: 10.1080/00268977600101031.
26. E. O. Pyzer-Knapp, H. P. G. Thompson, and G. M. Day. An optimized intermolecular force field for hydrogen bonded organic molecular crystals using atomic multipole electrostatics. *Acta Cryst. B*, 72:477–487, 2016.
27. Jonas Nyman, Orla Sheehan Pundyke, and Graeme M Day. Accurate force fields and methods for modelling organic molecular crystals at finite temperatures. *Physical Chemistry Chemical Physics*, 18(23):15828–15837, 2016.
28. L. X. Dang and B. M. Pettitt. A theoretical study of the inclusion complexes of β -quinol. *J. Chem. Phys.*, 89(2):968–974, 1988.
29. R. V. Belosludov, V. R. Belosludov, and V. E. Zubkus. The lattice dynamics of β -hydroquinone clathrate. *J. Chem. Phys.*, 103(8):2773–2778, 1995.
30. Y. N. Heit, K. D. Nanda, and G. J. O. Beran. Predicting finite-temperature properties of crystalline carbon dioxide from first principles with quantitative accuracy. *Chem. Sci.*, 7(1):246–255, 2016.
31. J. Nyman and G. M. Day. Modelling temperature-dependent properties of polymorphic organic molecular crystals. *Phys. Chem. Chem. Phys.*, 18:31132–31143, 2016. doi: 10.1039/C6CP05447A.
32. J. S. Tse, D. D. Klug, J. Y. Zhao, W. Sturhahn, E. E. Alp, J. Baumert, C. Gutt, M. R. Johnson, and W. Press. Anharmonic motions of Kr in the clathrate hydrate. *Nat. Mater.*, 4(12):917–921, 2005.
33. T. Matsuo. Phase transitions in the quinol clathrate compounds. II. The quinol methanol clathrate compound. *J. Phys. Soc. Jpn.*, 30(3):794–805, 1971.
34. S. Hirokawa, T. Imasaka, and T. Matsuo. Quantum effects on the orientational ordering of H₂S and D₂S molecules enclosed in β -quinol clathrate. *J. Phys. Soc. Jpn.*, 63(2):593–601, 1994. doi: 10.1143/JPSJ.63.593.
35. A. Gavezzotti. The calculation of molecular volumes and the use of volume analysis in the investigation of structured media and of solid-state organic reactivity. *J. Am. Chem. Soc.*, 105:5220–5225, 1983.
36. K. Nakano, K. Sada, Y. Kurozumi, and M. Miyata. Importance of packing coefficients of host cavities in the isomerization of open host frameworks: Guest-size-dependent isomerization in cholic acid inclusion crystals with monosubstituted benzenes. *Chem. Eur. J.*, 7(1):209–220, 2001. ISSN 1521-3765. doi: 10.1002/1521-3765(20010105)7:1<209::AID-CHEM209>3.0.CO;2-Y.
37. L. von Szentpály, I. L. Shamovsky, R. Ghosh, V. E. Zubkus, and E. E. Tornau. Computer simulation studies on β -quinol clathrates with various gases. Interdependence of host and guest molecules. *The Journal of Chemical Physics*, 101(1):683–692, 1994. doi: http://dx.doi.org/10.1063/1.468124.
38. S. Meccozzi and J. Rebek Jr. The 55% solution: A formula for molecular recognition in the liquid state. *Chem. Eur. J.*, 4(6):1016–1022, 1998. ISSN 1521-3765. doi: 10.1002/(SICI)1521-3765(19980615)4:6<1016::AID-CHEM1016>3.0.CO;2-B.
39. S. L. Price. Why don't we find more polymorphs? *Acta Cryst. B*, 69(4):313–328, 2013.
40. J. Nyman and G. M. Day. Static and lattice vibrational energy differences between polymorphs. *CrystEngComm*, 17:5154–5165, 2015. doi: 10.1039/C5CE00045A.
41. Graeme M. Day and Andrew I. Cooper. Energy-structure-function maps: Cartography for materials discovery. *Adv. Mater.*, page 1704944, 2017. ISSN 1521-4095. doi: 10.1002/adma.201704944. 1704944.
42. Josh E Campbell, Jack Yang, and Graeme M Day. Predicted energy-structure-function maps for the evaluation of small molecule organic semiconductors. *J. Mat. Chem. C*, 5(30):7574–7584, 2017.
43. Angeles Pulido, Linjiang Chen, Tomasz Kaczorowski, Daniel Holden, Marc A Little, Samantha Y Chong, Benjamin J Slater, David P McMahon, Baltasar Bonillo, Chloe J Stackhouse, et al. Functional materials discovery using energy-structure-function maps. *Nature*, 543(7647):657, 2017.
44. Julia A Schmidt, Joseph A Weatherby, Isaac Sugden, Alejandro Santana-Bonilla, Francesco Salerno, Matthew Fuchter, Erin Johnson, Jenny Nelson, and Kim Jelfs. Computational screening of organic semiconductors: exploring side-group functionalisation and assembly to optimise charge transport in chiral molecules. *ChemRxiv preprint*, 2021.
45. Anthony M. Reilly and Richard I. Cooper et al. Report on the sixth blind test of organic crystal structure prediction methods. *Acta Cryst. B*, 72(4):439–459, Aug 2016. doi: 10.1107/S2052520616007447.
46. D. E. Braun, T. Gelbrich, V. Kahlenberg, and U. J. Griesser. Solid state forms of 4-aminoquinoline – from void structures with and without solvent inclusion to close packing. *CrystEngComm*, 17(12):2504–2516, 2015.
47. Angeles Pulido, Linjiang Chen, Tomasz Kaczorowski, Daniel Holden, Marc A Little, Samantha Y Chong, Benjamin J Slater, David P McMahon, Baltasar Bonillo, Chloe J Stackhouse, et al. Functional materials discovery using energy-structure-function maps. *Nature*, 543(7647):657, 2017.
48. A. J. Cruz-Cabeza, G. M. Day, and W. Jones. Predicting inclusion behaviour and framework structures in organic crystals. *Chem. Eur. J.*, 15(47):13003–13040, 2009. ISSN 1521-3765. doi: 10.1002/chem.200901703.
49. AP Dianin. Condensation of phenol with unsaturated ketones. condensation of phenol with mesityl oxide. *J. Russ. Phys. Chem. Soc.*, 46:1310, 1914.
50. S.-P. Kang and H. Lee. Equilibrium dissociation pressures for p-cresol + methane and p-cresol + nitrogen clathrates at temperatures above the normal melting temperature of p-cresol. *J. Chem. Eng. Data*, 42(3):467–469, 1997. doi: 10.1021/je960360v.
51. René Clement, Charles Mazieres, and Lucien Guibe. Low temperature phase changes in the urea-trioxane inclusion compound. *Journal of Solid State Chemistry*, 5(3):436–440, 1972.
52. Maria M Ilczyszyn, Marek Ilczyszyn, and Marcin Selent. Structure and stability of p-cresol-xenon clathrate: Raman spectroscopy study. *Journal of Molecular Structure*, page 128147, 2020.
53. Michael Mastalerz, Stefanie Sieste, Miła Cenić, and Iris M Oppel. Two-step synthesis of hexammonium triptycene: an air-stable building block for condensation reactions to extended triptycene derivatives. *The Journal of organic chemistry*, 76(15):6389–6393, 2011.
54. M. Mastalerz and I. M. Oppel. Rational construction of an extrinsic porous molecular crystal with an extraordinary high specific surface area. *Angew. Chem. Int. Ed.*, 51(21):5252–5255, 2012. ISSN 1521-3773. doi: 10.1002/anie.201201174.
55. J. E. Mock, J. E. Myers, and E. A. Trabant. Crystallization of the rare-gas clathrates. *Ind. Eng. Chem. Res.*, 53(12):1007–1010, 1961.
56. Qiang Zhu, Alexander G Shtukenberg, Damien J Carter, Tang-Qing Yu, Jingxiang Yang, Ming Chen, Paolo Raiteri, Artem R Oganov, Boaz Pokroy, Iryna Polishchuk, et al. Resorcinol crystallization from the melt: a new ambient phase and new "riddles". *Journal of the American Chemical Society*, 138(14):4881–4889, 2016.
57. J. A. Ripmeester, C. I. Ratcliffe, and J. S. Tse. The nuclear magnetic resonance of 129Xe trapped in clathrates and some other solids. *J. Chem. Soc. Faraday Trans.*, 84(11):3731–3745, 1988.
58. Peter Bygrave and Graeme Day. Dataset for crystal structure prediction dataset for: resorcinol crystallization from the melt: A new ambient phase and new "riddles", 2016.
59. Q. Zhu, A. G. Shtukenberg, D. J. Carter, T.-Q. Yu, J. Yang, M. Chen, P. Raiteri, A. R. Oganov, B. Pokroy, and I. Polishchuk et al. Resorcinol crystallization from the melt: A new ambient phase and new "riddles". *J. Am. Chem. Soc.*, 138(14):4881–4889, 2016.
60. A. L. Spek. Platon, an integrated tool for the analysis of the results of a single crystal structure determination. *Acta Cryst. A*, 46:c34–c34, 1990.
61. T. F. Willems, C. H. Rycroft, M. Kazi, J. C. Meza, and M. Haranczyk. Algorithms and tools for high-throughput geometry-based analysis of crystalline porous materials. *Microporous Mesoporous Mater.*, 149(1):134–141, 2012.
62. P. van der Sluis and A. L. Spek. BYPASS: an effective method for the refinement of crystal structures containing disordered solvent regions. *Acta Cryst. A*, 46(3):194–201, Mar 1990. doi: 10.1107/S0108767389011189.
63. Leonard J Barbour. Crystal porosity and the burden of proof. *Chemical communications*, (11):1163–1168, 2006.
64. N. B. McKeown. Nanoporous molecular crystals. *J. Mat. Chem.*, 20(47):10588–10597, 2010.
65. S. L. Price, M. Leslie, G. W. A. Welch, M. Habgood, L. S. Price, P. G. Karamertzanis, and G. M. Day. Modelling organic crystal structures using distributed multipole and polarizability-based model intermolecular potentials. *Phys. Chem. Chem. Phys.*, 12:8478–8490, 2010. doi: 10.1039/C004164E.
66. J. Nyman, O. Sheehan Pundyke, and G. M. Day. Accurate force fields and methods for modelling organic molecular crystals at finite temperatures. *Phys. Chem. Chem. Phys.*, 18:15828–15837, 2016. doi: 10.1039/C6CP02261H.
67. Maurizio Cossi, Vincenzo Barone, Roberto Cammi, and Jacopo Tomasi. Ab initio study of solvated molecules: a new implementation of the polarizable continuum model. *Chemical Physics Letters*, 255(4-6):327–335, 1996.
68. M. J. Frisch, G. W. Trucks, H. B. Schlegel, G. E. Scuseria, M. A. Robb, J. R. Cheeseman, G. Scalmani, and V. Barone et al. Gaussian 09 Revision A.02, 2009. Gaussian Inc. Wallingford CT 2009.
69. D. E. Williams. Improved intermolecular force field for molecules containing H, C, N, and O atoms, with application to nucleoside and peptide crystals. *J. Comput. Chem.*, 22(11):1154–1166, 2001. ISSN 1096-987X. doi: 10.1002/jcc.1074.
70. D. E. Williams. Improved intermolecular force field for crystalline oxohydrocarbons including O-H...O hydrogen bonding. *J. Comput. Chem.*, 22(1):1–20, 2001.
71. A. J. Stone. Distributed multipole analysis of Gaussian wavefunctions. GMDA version 2.2.02.
72. Wei Zhang, Zihui Song, Michael T Ruggiero, and Daniel M Mittleman. Assignment of terahertz modes in hydroquinone clathrates. *Journal of Infrared, Millimeter, and Terahertz Waves*, pages 1–11, 2020.
73. Jonas Nyman, Lian Yu, and Susan M Reutzel-Edens. Accuracy and reproducibility in crystal structure prediction: the curious case of roy. *CrystEngComm*, 21(13):2080–2088, 2019.
74. G. M. Day, S. L. Price, and M. Leslie. Atomistic calculations of phonon frequencies and

- thermodynamic quantities for crystals of rigid organic molecules. *J. Phys. Chem. B*, 107 (39):10919–10933, 2003. doi: 10.1021/jp035125f.
75. G. M. Day. *Lattice Dynamical Studies of Molecular Crystals with Application to Polymorphism and Structure Prediction*. PhD thesis, University College London, 2003.
 76. B. W. Silverman. *Density estimation for statistics and data analysis*, volume 26. CRC press, 1986.
 77. A. M. Karo and J. R. Hardy. Lattice dynamics of NaF. *Phys. Rev.*, 181(3):1272, 1969.
 78. P. Debye. Zur theorie der spezifischen Wärmen. *Ann. Phys. (Berlin)*, 344(14):789–839, 1912.
 79. Jonas Nyman. *Computational predictions of structures, inclusion behaviour and properties of organic molecular crystals*. PhD thesis, University of Southampton, 2017.
 80. G. Gilat and L. J. Raubenheimer. Accurate numerical method for calculating frequency-distribution functions in solids. *Phys. Rev.*, 144(2):390, 1966.
 81. G. Gilat and B. J. Alder, editors. *Methods in Computational Physics*, chapter Methods of Brillouin zone integration. Number 15 in Advances in research and applications. Academic Press, 1976.
 82. Daan Frenkel and Berend Smit. *Understanding molecular simulation: from algorithms to applications*, volume 1. Elsevier, 2001.
 83. James Arvo. Fast random rotation matrices. In *Graphics Gems III (IBM Version)*, pages 117–120. Elsevier, 1992.
 84. Santiago Alvarez. A cartography of the van der waals territories. *Dalton Transactions*, 42 (24):8617–8636, 2013.
 85. Jonas Nyman and Susan M. Reutzel-Edens. Crystal structure prediction is changing from basic science to applied technology. *Faraday Discuss.*, 211:459–476, 2018. doi: DOI: 10.1039/C8FD90032A.
 86. Fokion Karavias and Alan L. Myers. Isotheric heats of multicomponent adsorption: thermodynamics and computer simulations. *Langmuir*, 7(12):3118–3126, 1991. doi: 10.1021/la00060a035.
 87. A. Kitaigorodsky. *Molecular crystals and molecules*, volume 29. Elsevier, 2012.
 88. Bo Guo, Liping Chang, and Kechang Xie. Adsorption of carbon dioxide on activated carbon. *Journal of Natural Gas Chemistry*, 15(3):223–229, 2006.
 89. Jarosław Serafin, Urszula Narkiewicz, Antoni W Morawski, Rafal J Wróbel, and Beata Michalkiewicz. Highly microporous activated carbons from biomass for CO₂ capture and effective micropores at different conditions. *Journal of CO₂ Utilization*, 18:73–79, 2017.
 90. Jerzy Choma, Kamila Stachurska, Michał Marszewski, and Mietek Jaroniec. Equilibrium isotherms and isotheric heat for CO₂ adsorption on nanoporous carbons from polymers. *Adsorption*, 22(4-6):581–588, 2016.
 91. Tsuyoshi Watabe and Katsunori Yogo. Isotherms and isotheric heats of adsorption for CO₂ in amine-functionalized mesoporous silicas. *Separation and Purification Technology*, 120: 20–23, 2013.
 92. HM Powell. The structure of molecular compounds. Part VII. Compounds formed by the inert gases. *Journal of the Chemical Society (Resumed)*, pages 298–300, 1950.
 93. Weiwei Zhang, Artem R Oganov, Alexander F Goncharov, Qiang Zhu, Salah Eddine Bouffelfel, Andriy O Lyakhov, Elissaios Stavrou, Maddury Somayazulu, Vitali B Prakapenka, and Zuzana Konôpková. Unexpected stable stoichiometries of sodium chlorides. *Science*, 342(6165):1502–1505, 2013.
 94. Helen E. Maynard-Casely, Robert Hodyss, Morgan L. Cable, Tuan Hoang Vu, and Martin U Rahm. A co-crystal between benzene and ethane: a potential evaporite material for Saturn's moon Titan. *IUCrJ*, 3(3):192–199, May 2016. doi: 10.1107/S2052252516002815.
 95. Stefan Habermehl, Philipp Moerschel, Pierre Eisenbrandt, Sonja M Hammer, and Martin U Schmidt. Structure determination from powder data without prior indexing, using a similarity measure based on cross-correlation functions. *Acta Cryst. B*, 70(2):347–359, 2014.
 96. Rajni M Bhardwaj, Jennifer A McMahon, Jonas Nyman, Louise S Price, Sumit Konar, Iain DH Oswald, Colin R Pulham, Sarah L Price, and Susan M Reutzel-Edens. A prolific solvate former, galunisertib, under the pressure of crystal structure prediction, produces ten diverse polymorphs. *Journal of the American Chemical Society*, 141(35):13887–13897, 2019.